- If certain design specifications are not met some parameters must be relaxed and iteration through the above procedure is called for.

8 Application of Tomography in Engineering Research

Although Computed Tomography (CT) has found extensive application in the medical field its use for engineering applications has been relatively recent and limited in range. It has been used mostly for nondestructive testing of materials, such as manufactured parts like turbine blades in the aerospace industry (Azevedo et al., 1993). A few cases, in which either tomography in its original form or its principles in combination with traditional measurement methods, appeear in the process engineering research literature and are briefly discussed below.

Yule et al. (1981) combined the measurements from a light scattering technique with the tomographic reconstruction process for the measurement of droplet size and concentration in an axisymmetric spray produced by an twin-fluid atomizer. A HeNe laser beam is passed through the spray and the forward scattered light is collected by a Fourier transform lens arrangement. Particles of the same diameter produce the same radial scattered light intensity which is measured by a photodetector. The scattered light that is measured is effectively a line integral along the laser beam traversing different paths through the spray. The use of Fraunhofer diffraction theory, in combination with a tomographic reconstruction process, provides a two dimensional distribution of particle sizes and concentrations in a plane across the spray. A similar approach has been used by Liu et al. (1989) who applied tomographic reconstruction methods to the speckle photographic measurements of an asymmetric flow field with variable fluid density. Hertz (1985) used a Mach-Zehnder interferometer for recording projections of the index of refraction in a two dimensional flame from eight different directions. The projections are used to reconstruct the 2-D distribution of the refractive index, and a relationship is then used for obtaining the temperature distribution from the refractive index distribution. The integral measurements through a turbulent Helium jet were obtained by Watt and Vest (1990) using pulsed, phase-shifting, holographic interferometry. Multiangular viewing of the holographic interferograms provided the data for using tomographic reconstruction of the jet's concentration field.

All the above studies primarily used the tomographic reconstruction process for the line integrals measured using optical techniques. There are a few studies on the application of CT for the characterization of flow through porous media. Hicks et al. (1990) used a commercial X-ray CT scanner for studying the heterogeneities of carbonate cores with the objective of targetting the bypassed oil in carbonate oil reservoirs for improved oil recovery.

The axis of the scanner was reoriented from its original design to make the scan plane horizontal. Porosity and residual oil saturation distributions were of interest in this study. A similar study of core analysis for determining the saturation and distribution of fluids using a commercial X-ray CT scanner was made by Coles et al. (1991) at Mobil's R & D center in Dallas. Jasti et al. (1990) used a cone-shaped diverging X-ray beam along with a two dimensional X-ray detector to directly obtain a three dimensional reconstruction of the flow through porous media. Their system consists of an X-ray tube whose focal spot size is in the range of 1-5 micrometers. The accelerating potential used is 60 kV and the two dimensional transmission image of the object is captured by a two dimensional X-ray detector. Instead of the source and the detector arrangement rotating around the object to be imaged, the object is rotated about its own axis. This arrangement would be suitable to use for imaging static systems and where it is convenient to do so, which is often not the case.

Reported research studies in the literature focusing on the use of CT for holdup or concentration distribution of phases in chemical reactors such as bubble columns and fluidized beds are far fewer. The ones that have been reported were most often concerned with demonstrating the feasibility of using CT for this purpose. In addition, different kinds of tomography have been used in these studies.

Hau and Banerjee (1981) applied a tomographic reconstruction of two sets of mutually perpendicular scans obtained from a densitometer for a horizontal two phase flow. Their equipment consisted of a 100 mCi Pu 238 source, and a sodium iodide scintillation detector. The source-detector arrangement is mounted on a traversing mechanism such that the attenuation measurements could be scanned along vertical and horizontal chords. Seven such chordal measurements in the vertical and horizontal direction, making up a total of 14, were used to reconstruct the mixture density distribution on a 7×7 matrix. The algorithm for reconstruction was based on the Algebraic Reconstruction Technique (ART).

At the Idaho National Engineering Laboratory Fincke et al. (1980) used tomography to determine the time averaged density and its distribution in horizontal multiphase flows. Unlike the study mentioned above the hardware that was designed was truly a tomographic scanner. The system had 9 detectors arranged in an arc. The source used was a 0.5 Ci Americium - 243 with a 60 keV gamma as the principal photopeak. The source is collimated into a fan beam with a subtended angle of 32°. The assembly of source and detector array rotates about the pipe center line on ball bearing assemblies. The reconstruction of the density distribution is based on the Algebraic Reconstruction Technique (ART). The test section was three inches in diameter. Based on the gradients in density distribution they were able to differentiate between flow regimes ranging from stratified flow to annular flow.

De Vuono et al. (1980) carried out a parametric analysis for arriving at an optimum design of a CT scanner for two phase flow studies. This paper serves as an excellent starting point for the design of a CT system. The parametric analysis allows one to arrive at design parameters based on the requirements set for the spatial and density resolution, the size of the test section to be scanned along with constraints on the maximum available count rate (source strength) and the allowable scan time (i.e., the desired temporal resolution). The analysis has been made with reference to the fourth generation scanning configuration wherein there is a large number of detectors all around the test section and it is only the source of radiation that rotates on a circle between the detectors and the test section. However, some of the principles can be well utilized for the design of systems in the third generation configuration as well.

The application of gamma ray tomography for voidage measurements in fluidized beds has been demonstrated by Seville et al. (1986). The scanning system that was developed for that purpose was simple consisting of a 100 mCi Americium - 243 source and a single collimated NaI detector. The source and the detector were aligned using an optical bench. The fluidized bed was mounted on a rotating table so that it can be moved linearly with respect to the beam for obtaining measurements along different chords, and also rotated about its axis to obtain the measurements at different angular orientations. The test section was 14.6 cm in diameter and the spatial interval for the chordal measurements was 5 mm. The chordal measurements were obtained at 30 different angular positions at intervals of 6°. The total time for data collection for scanning one section was 6 to 7.5 hours. Because of the simplicity of the system's hardware, and the consequent long scanning times, an extensive study was not undertaken. The objective of the study appeared to be the demonstration of the feasibility of using CT for voidage measurements in fluidized beds. The CT scans of the grid region of the bed were used to compare the experimentally determined jet entrance length with theoretical predictions. An improved version of the scanner from the same group is reported by Simons et al. (1993). The new system had six Gadolinium-153 sources with corresponding six collimated CsI scinitillation detectors. The assembly was mounted on a fixed rotation stage which had a central hole of 100 mm in diameter. The test section had to be lowered or raised through the scanning assembly so that different sections of the flow can be scanned. Each view consisted of a lateral translation in steps of 1.0 mm and each scan consisted of several views obtained by rotating the scanning assembly through 180° in steps of 1.5°. The reconstruction was done on a matrix of pixels 1 mm $\times$ 1 mm and the total scanning time was 3 to 4 hours. The scanner was used to study the differences in behavior of a spouted fluidized bed with dry and sticky particles in terms of the penetration of the inlet jet as well as the voidage profiles. This system has also been used by Ashrafi and Tuzun

(1993) for studying the granular flow of solids in a model hopper rig. The scanning time for each section is reported to have been reduced to 90 seconds. Contrary to the earlier system, in the refined system the scanning assembly rotates around the test section. The maximum size of the test section that could be scanned is 100 mm and the Filtered-Backprojection algorithm is reportedly used for image reconstruction. The cross-sectional profiles of solids fraction at different heights, as well as the plane mean values of void fraction, were obtained in both the cylindrical and conical sections of the hopper.

Banholzer et al. (1987) conducted a feasibility study for direct imaging of time averaged flow patterns in a model fluidized bed reactor using X-ray tomography. Essentially, a model fluidized bed (150 mm long, and 43 mm inside diameter) containing powdered coal was scanned using a medical CT scanner under a range of experimental conditions. The scanner made use of a 88-kW X-ray tube and an array of 517 gas filled X-ray detectors on the opposite side. The X-ray beam was collimated to a 1500 μm thick fan beam with an included angle of 30 degrees. The system was capable of scanning a section in 9 seconds. A spatial resolution of 1.5 mm and a density resolution of better than 30 kg/m^3 were achieved. No mention is made about the algorithm used for image reconstruction. Considering that the system used was a medical scanner the algorithm was probably the convolution-backprojection method.

Lutran et al. (1991) used a medical CT scanner for visualizing the liquid distribution in trickle beds with a quiescent gaseous phase. The test section was square, with a side of 7.3 cm and a height of only 30.48 cm, so that it was convenient to use a medical scanner and image the longitudinal sections of the bed. As in some of the earlier studies it appears that the dimensions of the test section in which the flow was studied were dictated by the largest scannable section (patient) by the scanner. Again since the system was a commercial scanner nothing was discussed about the hardware and the software for image reconstruction. The system was used to study the effects of liquid flow rate, prewetting, particle size, inlet configuration, surface tension and flow history on the flow pattern in the packed bed.

Kantzas (1994) used a EMI 7070 commercial X-ray CT scanner for obtaining the holdup distribution in fluidized and trickle beds. The scanner is of the fourth generation type and being a medical scanner it was modified to perform scans in both the horizontal and vertical direction. The system is capable of completing a scan for one section in 3 seconds. Spatial resolution of 0.4 cm $\times$ 0.4 cm is claimed. No mention is made about the reconstruction procedures. The fluidized bed studied was a glass bead - nitrogen system in a column of 10.0 cm in diameter. The gas was introduced in to the bed by a distributor plate with a long orifice in the center. A series of images as a function of time and position have been presented. The scans over the orifice tip showed the formation of a jet and a thin high-density ring surrounding the expanding jet corresponding to the high concentration of solids

around the jet. The trickle bed used in the study was a glass bead - nitrogen - water system in a glass column of 0.045 m diameter and 0.45 m length. The holdup of the liquid and gas phase under three phase conditions was calculated based on the scans made of the dry bed, a liquid saturated bed and the use of relativity principles.

X-ray tomography was used by Toye et al. (1994) for imaging the gas-liquid-solid distribution in trickling filters. The system consists of a point source X-ray generator that produces a fan beam with an included angle 0f 40°. The X-ray energy could be varied from 0 to 160 kV. The detector used was a linear array of 1024 photodiodes, so that effectively there were 1024 projections within the fan beam. The bed scanned had a diameter of 0.6 m and was 2m in height. A Fourier based algorithm for reconstruction was adopted. The reconstruction was done on a matrix of 1024 $\times$ 1024 pixels. The liquid holdup in the bed is claimed to be detected inspite of the low liquid film thickness around the packed solids.

9 Experimental Results for Void Fraction Distribution in a Bubble Column

We end our discussion of the research applications of tomography by presenting here some results on the void fraction distribution in bubble columns that were obtained using the CT scanner in our laboratory. Comparison of the void fraction results obtained using the CT scanner with results in the literature and with the data obtained using other techniques are presented in Kumar et al. (1995), and Kumar (1994). In this section the results for the effect of operating conditions on the void fraction and its distribution in bubble columns are discussed. Experiments were performed in bubble columns of five different diameters (0.102, 0.14, 0.19, 0.26 and 0.30 m) using air and mainly tap water as the gas and liquid phase, respectively. Four superficial gas velocities - 0.02 m/s, 0.05 m/s, 0.08 m/s and 0.12 m/s - were used for most of the columns. These velocities cover all the flow regimes from bubble to churn turbulent in all the columns. For all the column sizes the experiments were conducted with a static liquid height to diameter ratio of at least 5. All the runs were made with zero liquid superficial velocity. The data was obtained mainly in columns fitted with a perforated plate distributor. The distributors were made out of 0.0032 m thick aluminum plates. The open area of the distributors ranged from 0.05 to 0.23 %. The characteristics of the hole patterns and their sizes for the different columns can be found in Kumar (1994). To evaluate the effects of gas distribution, the flow in the 0.19 m diameter bubble column was imaged with two other types of gas distributors in addition to the perforated plate. These were a simple cone and a single bubble cap riser. For most of the runs the scans were performed at five different elevations above the distributor for capturing the evolution

of void distribution with flow development. Most of the results reported here are the void fraction profiles that have been averaged over those sections of the flow for which the end (i.e., entry and disengagement sections of the flow) effects are negligible.

Effect of Column Diameter

The effect of column diameter on the void fraction distribution is shown in Fig. 11 (a) and (b) for superficial gas velocities corresponding to flow in the bubbly and churn turbulent flow regimes. The void profiles are from scans of the columns at a section where end effects are negligible. At the low gas flow rate ($U_g = 0.2\,m/s$) it is evident that there is some influence of the column diameter on the void fraction although there appears to be no specific trend. In churn turbulent flow at the gas flow rate corresponding to $U_g = 0.08\,m/s$

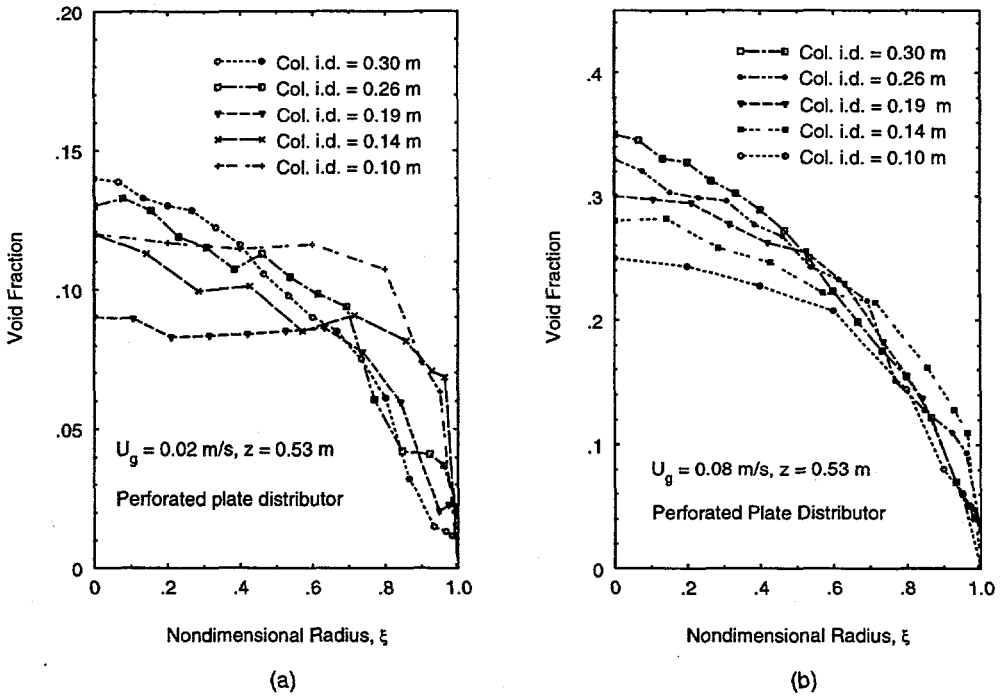

Figure 11: Effect of column diameter; (a) $U_g = 0.02\,m/s$, (b) $U_g = 0.08\,m/s$

there is a continuous increase in the void fraction with column diameter. The integral area under the curves were computed to evaluate the cross-sectional mean void fraction. These are tabulated in Table 4. At the low gas velocity the cross-sectional mean void fraction decreases initially with the column diameter and then increases again. At the higher gas velocity the holdup values continuously increase with the column diameter, although this increase tapers off gradually. This observation is in line with the observation made in the

literature that the overall gas holdup is unaffected by the column diameter provided it is greater than 0.15 m.

Table 4: Cross-Sectional mean void fraction as a function of column diameter

Column i.d. - m	X-Sect. Mean Void Fraction	
	$U_g = 0.02 m/s$	$U_g = 0.08 m/s$
0.10	0.106	0.191
0.14	0.094	0.209
0.19	0.075	0.225
0.26	0.095	0.234
0.30	0.104	0.238

Effect of Superficial Gas Velocity

The effect of superficial gas velocity on the void fraction distribution is illustrated in two of the columns studied. Fig. 12 (a) and (b) correspond to the void fraction distributions obtained in the 0.10 m and 0.26 m diameter columns as a function of superficial gas velocity. The data correspond to scans at one fixed axial location that is well away from entrance or free surface effects. In general, an increase in the gas velocity leads to an increase in the magnitude of the local void fraction at all column radii except at regions close to the wall. The magnitude of this increase is much larger at the lower velocities corresponding to the bubbly and transition flow regimes. At the higher velocities (churn turbulent flow) the increase is relatively small. The holdup profile changes from a flatter distribution to a more parabolic one with increase in the superficial gas velocity.

Effect of Distributor Type

The effect of the type of distributor used on the void fraction distribution was studied in the 0.19 m diameter column. Three different kinds of distributors were used. The first of these was a perforated plate having 156 holes on a square pitch of 1.25 cm leading to an open area of 0.1 %. The second was a cone distributor and the third distributor used was a bubble cap. Their geometrical characteristics are illustrated in Fig. 13.

The cross-sectional distribution of the void fraction distribution shown in Fig. 14 clearly shows the differences resulting from the distributors. It is seen that the perforated plate results in a uniform distribution of the gas and this gets reflected in the gradual variation in the colors for the void fraction from the column center to the wall. For the cone and

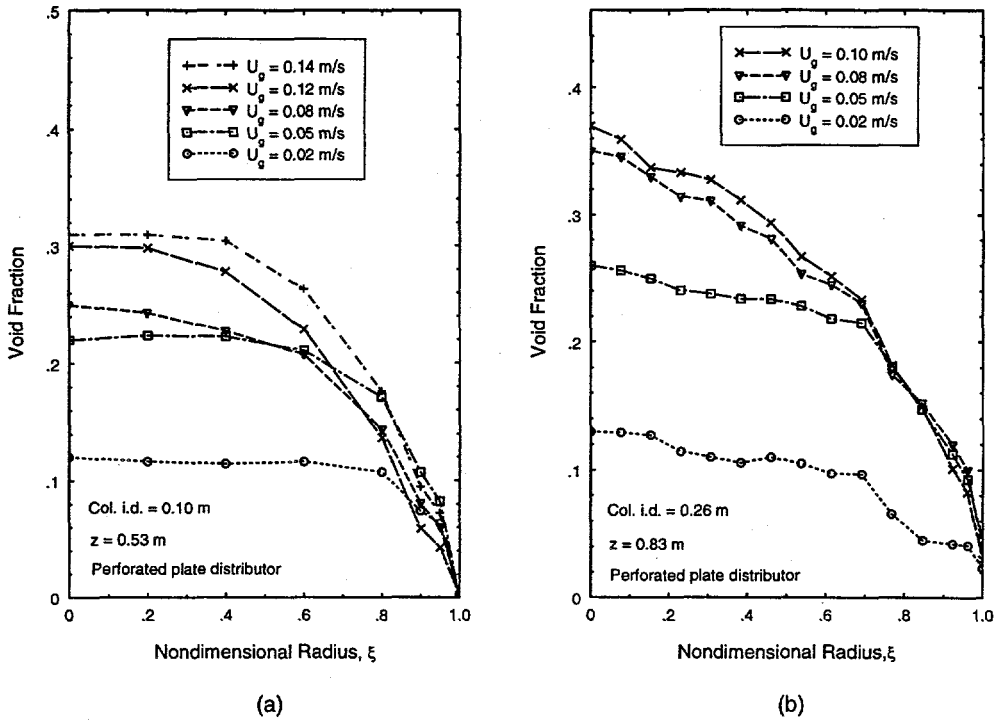

Figure 12: Effect of superficial gas velocity; (a) Col. i.d. = 0.10 m, (b) Col. i.d. = 0.26 m

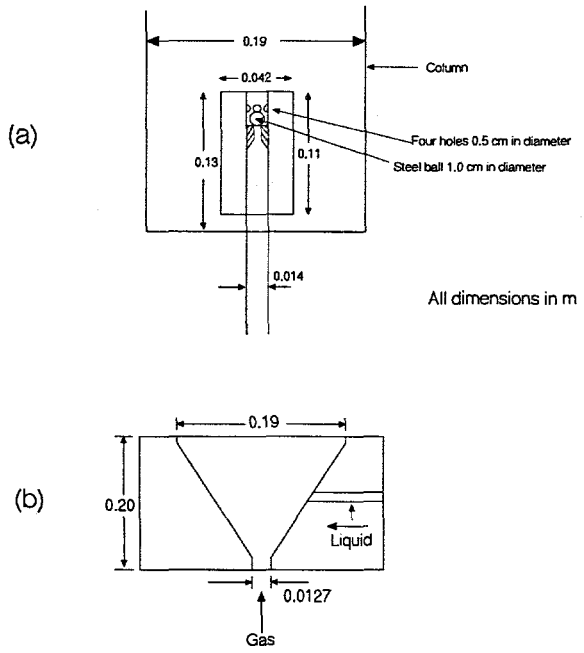

Figure 13: Characteristics of (a) Bubble cap, (b) Cone distributor

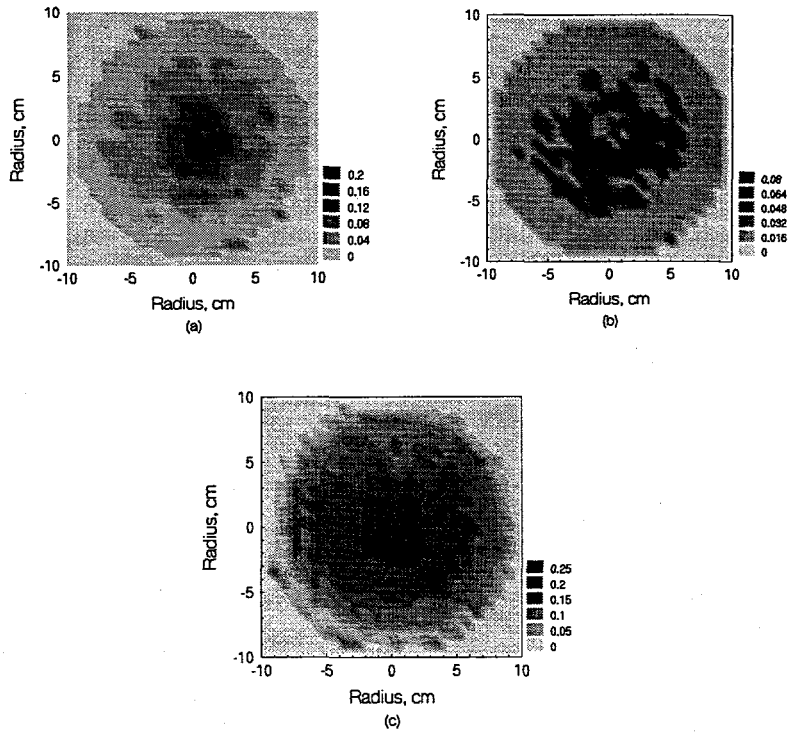

Figure 14: Void fraction distribution from three distributors; Col. i.d. = 0.19 m; z = 0.83 m; U_g = 0.04 m/s; Distributor : (a) Bubble Cap, (b) Cone, (c) Perforated plate

the bubble cap distributors the gas moves up the column as large bubbles in a region close to the column center. The peripheral regions are almost unaerated and this is reflected as an annulus of light shades in the cross-sectional image. At the higher gas velocities these differences get minimized owing to the breakup of the large bubbles due to the higher intensity of turbulence generated at these flow rates.

It is common in academic research to use a sintered plate distributor. The comparison of such a distributor and a perforated plate distributor was studied in the 0.10 m diameter column. The liquid phase used was a mixture of isopropanol and water mixed in equal volumes. The comparison between the void profiles resulting from the two kinds of distributors are shown in Fig. 15. This mixture resulted in very fine bubbles and at high velocities also led to excessive foaming especially with the sintered plate distributor. The magnitude of the holdup generated by the sintered plate is larger than that of the perforated plate and this difference increases with increase in gas velocity. At $U_g = 0.8\,m/s$ the foaming tendency with the sintered plate distributor is very well discerned by the CT scanner.

Effect of Liquid Properties

The effect of using highly purified and deionized water against regular tap water was studied in the 0.14 m diameter column. The deionized water was obtained from a compact

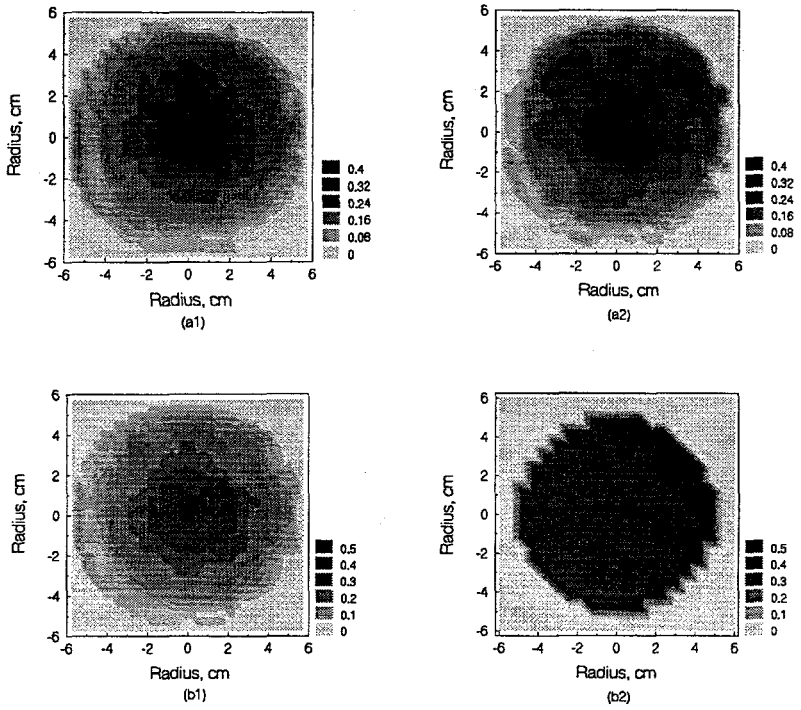

Figure 15: Void fraction distribution from sintered plate and perforated plate distributor; Col. i.d. = 0.10 m; z = 1.0 m; (a1, a2) $U_g = 0.04\,m/s$; (b1,b2) $U_g = 0.08\,m/s$; (a1,b1) perforated plate; (a2,b2) sintered plate

Milli-Q Plus water purification system that produces Type I reagent-grade water with a resistivity of 18 megohm-cm. The column, the distributor and the plenum were all washed with the same water before the actual runs. The void fraction distribution obtained from the CT scans of the column at an axial distance of 0.6 m above the distributor are shown in Fig. 16 for two different superficial gas velocities. The magnitude of the void fraction with the deionized water is always lower than that obtained with regular tap water. The bubble sizes observed in the column with deionized water were much larger and consequently, the holdup in the former is lower. These observations are consistent with the results of Anderson and Quinn (1978) who contend that the pure water promotes coalescence of the bubbles.

The effect of liquid physical properties was also studied by comparing the void distributions obtained with tap water and a mixture of tap water and isopropanol mixed in equal volumes. The isopropanol-water mixture had a viscosity of 0.00278 kg/m-s at 26°C, a surface tension of 28.2×10^{-7} N/m and a density of $917\,kg/m^3$. The bubble sizes observed in the mixture were small and of the order of 1 to 2 mm. This leads to extremely high values of the void fraction. The comparison between the two cases is depicted in Fig. 17.

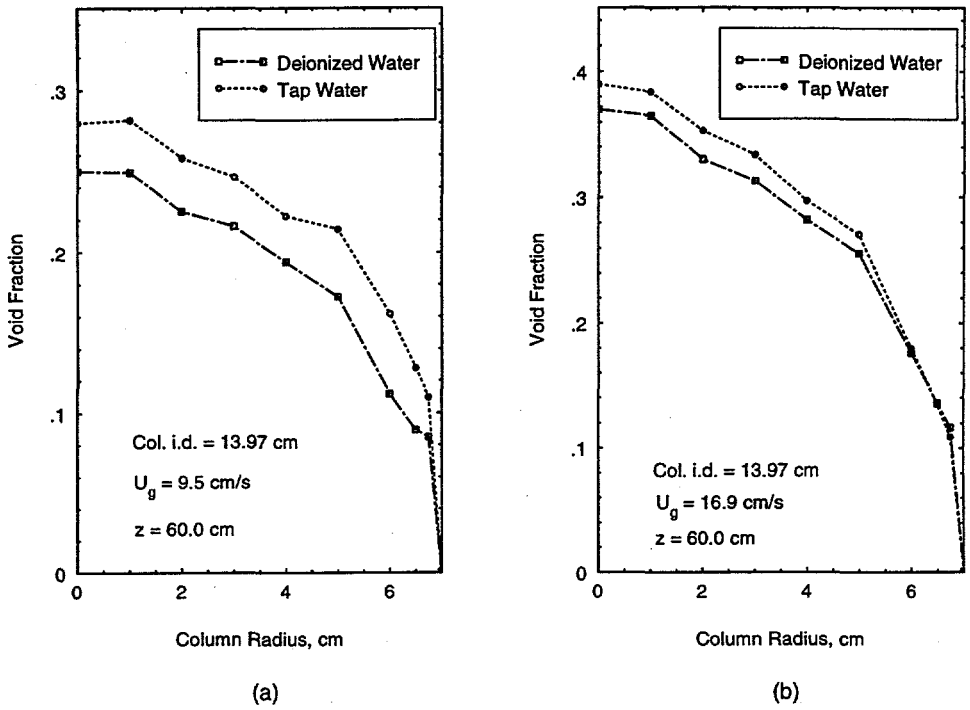

Figure 16: Effect of liquid properties - tap water and deionized water ; Col. i.d. = 0.14m, (a) $U_g = 0.038\,m/s$, (b) $U_g = 0.169\,m/s$.

10 Process Applications of Tomography

Use of tomography to study industrial scale reactors has not been reported to the best of our knowledge. This is primarily because of the complexity involved in setting up a CT system around an installed reactor. Space constraints and the existence of other structures in the vicinity such as flanges, piping, platforms, other auxiliary equipment and structures are the impediments for accomplishing a complete CT scan. In addition, the cost of obtaining the data for a complete scan is often prohibitive and its justification is considered difficult. However, a popular diagnostic tool in the chemical and process industry, executed by a number of small specialized companies, is commonly referred to as "gamma scanning". In its simplest form it was originally conceived as a diagnostic tool in the chemical and process industry. In its simplest form it was originally conceived by Du Pont in the 1960s (Severance, 1981) and has been subsequently improved and widely used (Severance, 1985; White, 1987; Harrison, 1990). In particular this technique has been extensively used for trouble shooting on distillation columns. The information obtained is used to detect the dislocation of trays, extent and location of tray flooding, liquid levels on aerated trays, location and characteristics of foaming, entrainment conditions etc. Essentially the attenuation of radiation of a single beam of radiation (probably along the centerline) is obtained as a function of axial position along the column. The signature profiles for an empty column, a normally operating column,

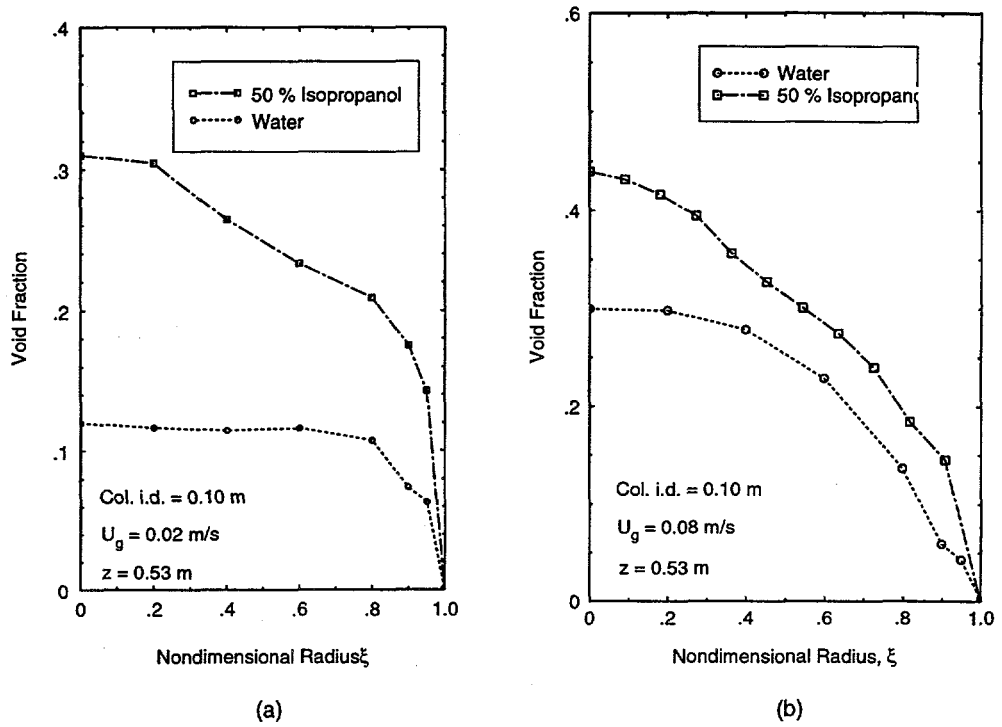

Figure 17: Effect of liquid properties - water and water-isopropanol mixture ; Col. i.d. = 0.10 m, (a) $U_g = 0.02 m/s$, (b) $U_g = 0.08 m/s$.

a flooded column etc. are established and then compared with the actual scan and used for problem diagnosis. Thus, the scan profiles are used as a visual representation of the hydraulic condition of the distillation column.

These simpler radiation techniques are finding great patronage by the chemical and process industry in the U.S. judging by the proliferation of companies that offer to provide such measurements as service. In recent years these companies provide what is known as two angle gamma scanning, which is the same as gamma ray densitometry. A gamma ray source on one side of the reactor and a radiation detector on the other side are mounted and a series of measurements for the attenuation of a narrow beam of radiation along several chords are obtained. This is then repeated at right angles to the first set of measurements by reorienting the source-detector arrangement. By identifying those paths in each set of measurements along which the attenuation is either maximum or minimum, it is claimed that the location and extent of the problem areas can be determined. To demonstrate that this is not necessarily true, we consider a reactor in which the cross-sectional distribution of gas holdup is represented (for illustrative purposes) by a 4 × 4 matrix of numbers as indicated in Fig. 18. The two angle scans are simulated by assuming that the initial number of photons is 10,000 and that each pixel in the matrix has unit length. Using the Beer-Lambert's law (assuming an ideal situation) the measured count rates for four individual beams at two positions that are 90 degrees apart are shown in Fig. 18. If the above described procedure is applied to

the two scans one would conclude that the highest holdup of the less dense phase (gas) lies at the intersection of the beams with the highest count rates and the lowest holdup at the intersection of beams with the lowest count rates. By using this argument in this simulated case the conclusion would be that the lowest holdup of the less dense phase (gas) should be in the pixel at the intersection of the fourth beam from left in the vertical direction and the third beam from the top in the horizontal direction which has a holdup of 0.2. Actually, the

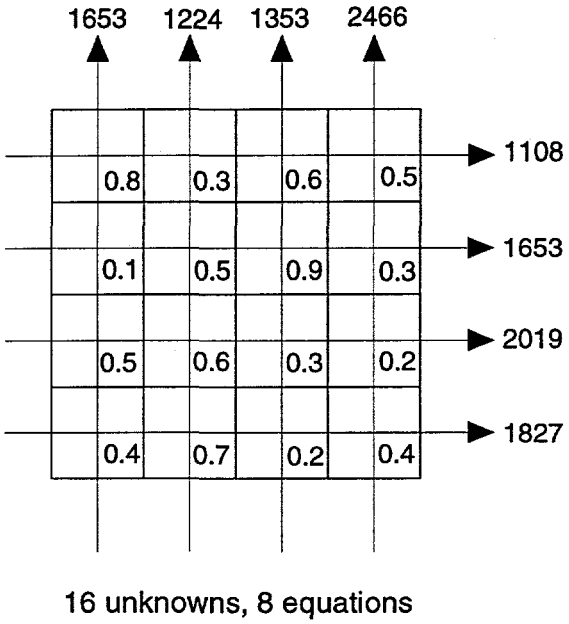

Figure 18: Gamma scan at two right angles

lowest holdup of 0.1 lies in another pixel that is not traversed by these beams. Similarly, the highest holdup using this interpretation would be given by the pixel at the intersection of the second beam from the left in the vertical direction and the first beam from the top in the horizontal direction. This pixel has a holdup of 0.3 while the maximum holdup in the distribution is 0.9.

The reason for the failure of the above described procedure to identify regions of highest or lowest holdups lies in having fewer equations than unknowns. Mathematically, one would require at least 16 independent attenuation measurements in order to determine the 16 unknown holdups (one in each cell) so that one has to obtain the measurements corresponding to at least two other angular orientations of the source-detector arrangement with respect to the reactor. Even with 16 measurements the distribution cannot be uniquely determined, since it is always possible to find a suitable combinations of numbers to satisfy the constraints set by the attenuation measurements. Theoretically speaking, for an accurate reconstruction an infinite number of measurements are required, which of course is not practically feasible.

However, the above example demonstrates that a set of two measurements at right angles lead to misleading conclusions, and one would require a reasonable number of such sets of measurements to make a diagnosis.

For industrial systems it is convenient and less expensive to obtain a few chordal measurements of the attenuation through the test section. Unfortunately, it is often forgotten that a single line averaged holdup, even if it is obtained across the centerline of the column is not representative of the cross sectional mean. The line averaged holdups along several chordal positions can, however, be used to obtain a cross-sectional mean provided that one assumes that the holdup distribution is axisymmetric. If such an assumption can be made, the radial variation of the holdup and, hence, the cross-sectional mean can be obtained by making use of the Abel integral and its inversion.

If f(r,R) is a function of radial position that is nonzero only within a circle of radius R, then its Abel transform is

$$\phi(x,R) = 2\int_0^{\sqrt{(R^2-x^2)}} f\left(\sqrt{(x^2+y^2)},R\right)dy = 2\int_x^R \frac{f(r,R)\,r}{\sqrt{r^2-x^2}}\,dr \qquad (19)$$

The above is merely the line integral along the ray in the y direction at the position x in the x-y coordinate system. The inversion expressing f in terms of ϕ is

$$f(r,R) = -\frac{1}{\pi}\int_r^R \frac{d\phi/dx}{\sqrt{x^2-r^2}}\,dx \qquad (20)$$

For our case, the quantity $\phi(x,R)$ corresponds to the quantity $ln(I_\circ/I)$ divided by the corresponding chordal length. Many different numerical approaches have been suggested for the implementation of the Abel inversion (Bockasten, 1961, W. L. Barr, 1962, Dong and Kearney, 1991). To illustrate that the centerline averaged holdup is an overestimate of the cross-sectional mean, and that the Abel inversion provides a radial distribution that leads to the correct cross-sectional mean, the following simulation has been made. An axisymmetric distribution of the holdup is assumed in an air-water bubble column of 19.05 cm in diameter. The assumed radial distribution has the functional form (Kumar, 1994)

$$\epsilon(\xi) = \bar{\epsilon}\frac{m+2}{m}(1-c\xi^m) \qquad (21)$$

where $\bar{\epsilon}$ is the cross-sectional mean holdup, m is the power law exponent and c is a constant that provides for non-zero holdup at the wall of the column. These parameters were obtained from the experimentally determined void fraction distributions using the CT scanner at CREL. The value of the power law exponent is high for a flat holdup distribution (corresponding to bubbly flow) and decreases for the more parabolic profile that is observed in

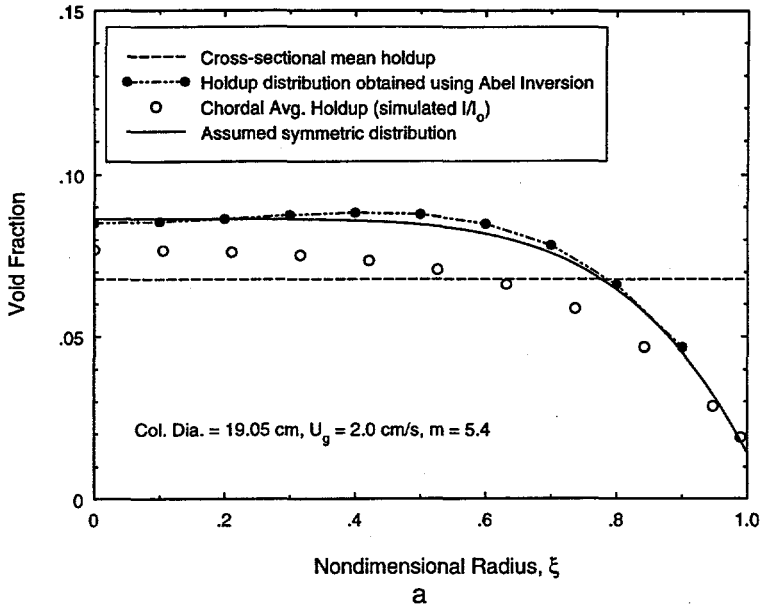

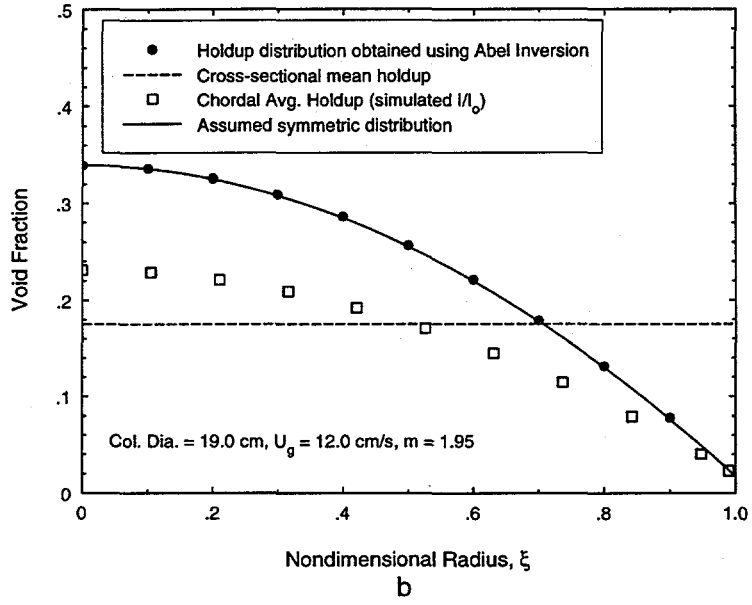

Figure 19: Comparison of assumed distribution, chordal averages and Abel inversion, (a) Bubbly flow, (b) Churn turbulent flow

churn turbulent regime. For a given holdup distribution the line integrals corresponding to the quantity $\int \left(\mu_{\text{air}}\,\epsilon + \mu_{\text{water}}\,(1-\epsilon)\right)\,dl$ are computed. The limits of integration depend on the position of the chord. The negative exponential of this quantity would correspond to the ratio $I\,/\,I_o$ that is measured in densitometry (as well as CT). Shown in Figures 19 (a) and (b) are the assumed symmetric holdup distributions (similar to experimentally determined holdup profiles in the two flow regimes), and the chordal average holdups that are obtained from the simulated line integrals for two values of m corresponding to bubbly and churn turbulent regimes, respectively. Also shown as a horizontal line for comparison is the cross-sectional mean. The chordal averaged centerline holdup is always higher than the cross-sectional mean. Using the entire set of chordal measurements, the Abel inversion pro-

vides a radial distribution that is the same (within numerical error) as the assumed (original) axisymmetric distribution. Abel inversion yields reliable results only when the distribution is axisymmetric. For industrial systems the current measurement practice can be modified to provide the chordal average measurements at two positions at right angles to each other. An assessment can than be made whether the assumption of axisymmetry is appropriate and if so a cross-sectional mean using Abel inversion can be obtained.

11 Recommendations for Improvements in Gamma-Ray Scanning of the AFDU Reactor at LaPorte

We conclude this report by providing guidelines for enhancing the measurements of holdup on the AFDU reactor at LaPorte using the nuclear density gauge. At present the instrumentation is being used for the measurement of only the chordal average holdup along the centerline of the reactor. It is recommended that for a given cross section the measurements be obtained along several such chordal positions at a minimum of two angular orientations (90° apart) with respect to the reactor. For the reactor of 18 inches in diameter it would be ideal to have a minimum of 12 chordal measurements across the section. This we believe is the least that has to be done and can be accomplished with minimal effort. Since the system is actually a three phase system it is desirable to resolve the concentration distribution of the three phases individually, and for this one has to resort to dual energy scanning. To accomplish this a gamma ray source with emissions at an energy different from that of the existing Cs-137 (0.66 MeV) source is required. Two possible options are Americium-241 (0.0595 MeV) and Cobalt-60 (1.17 MeV & 1.33 MeV). Although, the ideal choice for the second source is Am-241, the attenuation at this low energy of the source in a relatively large diameter system is high, and it becomes necessary to collect the data over long periods of time in order to obtain statistically significant photon count rates. Thus, the higher energy level emissions from Co-60 would appear to be a better choice. However, the attenuation coefficients of typical materials at the energy levels of Cs-137 and Co-60 are not vastly different to enable a clear resolution of the individual phases. This is because the calculated values of the phase holdups are very sensitive to small errors in the count rate measurements. Table 5 lists the linear attenuation coefficients of air, water and glass at four energy levels. If Co-60 is used as the second source, then it is better to gate in on the 1.33 MeV photopeak since that provides a wider difference in the attenuation coefficients with respect to the energy level of Cs-137. This off course requires additional hardware in the signal processing train to be able to differentiate between the photons at the two energy levels.

Finally we provide a design for what we call as the "Poor Man's Tomograph". The system

Table 5: Linear Attenuation Coefficient of some materials as a function of energy

Material	$\mu - cm^{-1}$ at 0.06 MeV	$\mu - cm^{-1}$ at 0.66 MeV	$\mu - cm^{-1}$ at 1.17 MeV	$\mu - cm^{-1}$ at 1.33 MeV
Air	2.14E-4	9.29E-5	7.67E-5	6.81E-5
Water	0.197	0.0857	0.0662	0.0619
Glass	0.5625	0.1942	0.1485	0.1387

is referred to by this title, since having a sophisticated CT system capable of providing fine spatial resolution is expensive and not practical for use on an industrial scale reactor. Thus, the system that we propose to be implemented for the reactor at LaPorte is capable of a spatial resolution of 3.0 cm $\times$ 3.0 cm, and does not require too long a period of time for scanning (considering the size of the reactor) and also is relatively simple in construction.

The system proposed here is novel in the sense that it combines the fan beam scanning configuration with the parallel beam scanning configuration. A schematic of the proposed scanning configuration is shown in Fig. 20. The arrangement consists of a source with the emissions collimated to a fan-beam with an included angle of about 20° and an array of three detectors whose centerlines are 5° apart. This assembly is designed to translate across the section for a given angular orientation with respect to the reactor. The idea here is that as the assembly traverses linearly across the section each detector is obtaining chordal measurements in separate views that are 5° apart. Once a linear scan is complete the whole assembly is rotated by 15° and the process is repeated until views over 180° have been obtained.

We follow the methodology for the design of a CT scanner set up in Section 7. The design is for a column of 61.0 cm (2 feet) inner diameter with a required spatial resolution of 3.0 cm $\times$ 3.0 cm. The preset parameters are :

1. $d_i = 61.0\,cm$ (column inner diameter)
2. $d_o = 63.5\,cm$ (column outer diameter)
3. $\Delta x = 3.0\,cm$ (spatial resolution)
4. $\sigma_\rho = 0.1\,g/cm^3$ (density resolution)
5. $S \leq 5\,Ci$
6. $N = 25 - 50$ counts / sec

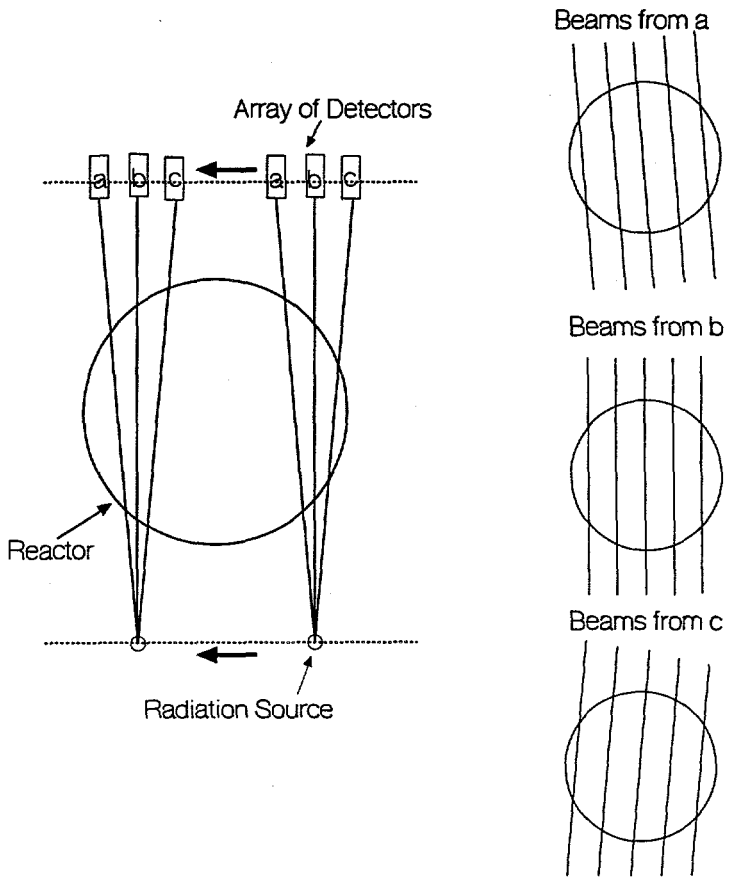

Figure 20: Schematic of the proposed scanning configuration

The assumptions are :

1. 180° scan
2. ϵ - detecting efficiency = 0.75
3. Energy level of photons : 0.66 MeV (Cs-137 source)
4. A maximum of 50 % solids loading with attenuation characteristics similar to glass.

For the required spatial resolution the collimators are designed to have rectangular apertures 3.0 cm × 1.5 cm. Using Eq. 16 the solid angle Ω is calculated as 0.0474. The column walls are assumed to be 0.5 inches thick and made of steel ($\rho\,\mu = 0.5678\,cm^{-1}$ at 0.66 MeV). With 50% solids loading the integral of the product $\mu\,l$ for all the material that the beam encounters along the center line of the reactor is 18.74. Using Eq. 15 the counting time required per beam (for the chosen count rate) with a 5 Curie source is calculated to be 40 seconds.

For a column of 2 feet in diameter with a required spatial resolution of 3.0 cm the number of chordal measurements required in one linear scan would be approximately 20 (number of

beams per view). However, from our experience with the CT measurements in our laboratory it seems appropriate to obtain half the above required number of chordal measurements and obtain the required number of beams by interpolating in between two measured beams. This is a reasonable method to adopt and aids in reducing the scanning time. The scanning time per view is therefore 40 seconds $\times$ 10 beams. The number of views required is calculated as 36. In the proposed methodology of scanning at any given time the data is being acquired for three views simultaneously. Hence, the required number of angular increments is 12, so that the total scanning time works out to be approximately 86 minutes.

The hardware for the support structure and the positioning mechanism can be made relatively simple and easy to install around a commercial reactor. Implementing such a system would go a long way in providing experimental information that definitely would serve in enhancing our understanding of the fluid dynamics of the system.

Implementing the dual energy scanning system with Co-60 as the additional source should be preceded by a preliminary study for evaluating if energy level differences between the emissions from Co-60 and Cs-137 is adequate for differentiating the three individual phases.

12 Nomenclature

A	absorptance of a medium
A_a	effective detector area
A_d	total detector area
d_a	actual detector aperture width
d_{eff}	effective detector aperture width
d_o	outer diameter of pipe
d_i	inner diameter of pipe
I	intensity of transmitted radiation
I_o	initial intensity of radiation
I_d	number detected photons
I_e	number emitted photons
l	path length of a beam of radiation through an object
L	total path length of radiation in a mixture of phases
m	total number of views per scan
M	magnification factor
n	number of beams or projections in a view
N	average number of photons per beam
	number of observations or samples
P	projection function in equation (4)

r	photon count rate - photons/sec
S_o	source strength - photons/sec
s	focal spot width of the source
T	transmittance, ratio of I to I_o
U_g	gas superficial velocity, m/s

Subscripts

w	water
p	pipe

Greek Symbols

Δx	spatial resolution
ϵ	detection efficiency
μ	mass attenuation coefficient, cm^2/g
Ω	Solid angle
ρ	material density, g/cm^3
τ	photon counting time
σ_ρ	density resolution

13 References

1. Anderson, J. L. and Quinn, J. A., 1970, "Bubble Columns : Flow Transitions in the Presence of Trace Contaminants", *Chem. Eng. Sci.*, Vol. 25, No. 3, pp. 373-380.

2. Ashrafi, M. E. H. and Tuzun, U., 1993, "A Tomographic Study of Voidage Profiles in Axially Symmetric Granular Flows", *Chem. Eng. Sci.*, Vol. 48, No. 1, pp. 53-67.

3. Azevedo, S. G., Schneberk, D. J., Fitch, J. P. and Martz, H. E., 1990, "Calculation of the Projection Centers in Computed Tomography Sinograms", *IEEE Trans. on Nucl. Sci.*,

4. Azevedo, S. G., Martz, H. E., and Schneberk, D. J., 1993, "Potential of Computed Tomography for Inspection of Aircraft Applications", *Int. Soc. for Optical Engg., Proc. of SPIE - Nondestructive Inspection of Aging Aircraft*, Vol. 2001, pp. 47-57.

5. Barr, W. L., 1962, "Method for Computing the Radial Distribution of Emitters in a Cylindrical Source", *J. Opt. Soc. Am.*, Vol. 52, No. 8, pp. 885-888.

6. Barrett, P. R., 1974, "Systematic Errors in the Discrete Time-Interval Transmission Method for the Estimation of Void Statistics in Boiling Channels", *Nucl. Eng. Des.,* Vol. 30, pp. 316-327.

7. Banholzer, W. F., Spiro, C. L., Kosky, P. G. and Maylotte, D. H., 1987, "Direct Imaging of Time-Averaged Flow Patterns in a Fluidized Reactor Using X-Ray Computed Tomography", *Ind. Engg. Chem. Res.*, Vol. 26, pp. 763-767.

8. Bockasten, K., 1961, *J. Opt. Soc. Am.*, Vol. 51, pp. 943.

9. Brooks, R. A. and Di Chiro, G., 1976, "Principles of Computer Assisted Tomography (CAT) in Radiographic and Radioisotopic Imaging", *Phy. Med. Biology*, Vol. 21, No. 5, pp. 689-732.

10. Coles, M. E., Muegge, E. L. and Sprunt, E. S., 1991, "Application of CAT Scanning for Oil and Gas Production Research", *IEEE Trans. on Nucl. Sci.*, Vol. 38, No. 2, pp. 510-515.

11. Daily, W. and Ramirez, A., 1995, "Environmental Process Tomography in the United States", *Chem. Eng. J.*, Vol. 56, No. 3, pp. 159-165.

12. Del Grande, Dolan, N. K., Durbin, K. W., Gorvad, P. F., Kornblum, M. R., Perkins, B. T., Schneberk, D. E., Shapiro, D. J. and Arthur B.", 1993, "Three-Dimensional Dynamic Thermal Imaging of Structural Flaws by Dual-Band Infrared Computed Tomography", *Int. Soc. for Optical Engg., Proc. of SPIE - Underground and Obscured Object Imaging and Detection*, Vol. 1942, pp. 207-215.

13. Dempster, A. P., Laird, N. M. and Rubin, D. B., 1977, "Maximum Likelihood Estimates from Incomplete Data via the E-M Algorithm", *J. Roy. Statis. Soc.*, Vol. 39, "Series B, pp. 1-38.

14. De Vuono A. C., 1979, *Design of a Computerized Tomographical Scanner Applied to Two Phase Flow Studies for Nuclear Reactor Safety Analysis*, Masters Thesis, Ohio State University, Columbus, OH,

15. De Vuono A. C., Schlosser, P. A., Kulacki, F. A. and Munshi, P., 1980, "Design of an Isotopic CT Scanner for Two Phase Flow Measurements", *IEEE Trans. on Nucl. Sci.*, Vol. NS-27, No. 1, pp. 814-820.

16. Dickin, F. J. Williams, R. A. and Beck, M . S., 1993, "Determination of Composition and Motion of Multicomponent Mixtures in Process Vessels Using Electrical Impedance

Tomography - I. Principles and Process Engineering Applications", *Chem. Emg. Sci.*, Vol. 48, pp. 1883-1897.

17. Dong, J. and Kearney, R. J., 1991, "Symmetrizing, Filtering, and Abel Inversion using Fourier Transform Techniques", *J. Quant. Spectrosc. Radiat. Transfer*, Vol. 46, No. 3, pp. 141-149.

18. Dreike, P. and Boyd, D. P., 1976, "Convolution Reconstruction of Fan-Beam Projections", *Comput. Graphics Image Processing*, Vol. 5, pp. 459-469.

19. Fincke, J. R., Berggren, M. J. and Johnson, S. A., 1980, "The Application of Reconstructive Tomography to the Measurement of Density Distribution in Two-Phase Flow", *Proc. of the 26 th International Instrumentation Symposium, Seattle*, pp. 235-243.

20. Glover, G. H. and Eisner, R. L., 1979, "Theoretical Resolution of Computed Tomography Systems", *J. Comput. Assist. Tomography*, Vol. 3, pp. 85-91.

21. Gordon, R., 1974, "A Tutorial on ART", *IEEE Trans. on Nuclear Science*, Vol. NS-21, No. 3, pp. 78-93.

22. Gordon, R. and Herman, G. T., 1974, "Three Dimensional Reconstruction from Projections - A Review of Algorithms", *Int. Rev. of Cytology*, Vol. 38, pp. 111-151.

23. Harrison, M. E., 1990, "Gamma Scan Evaluation for Distillation Column Debottlenecking", *Che. Eng. Prog.*, No. 3, pp. 37-44.

24. Hau, F. L. and Banerjee, S., 1981, "Measurement of Mass Flux in Two-Phase Flow Using Combinations of Pitot Tube s and Gamma Densitometry", *AIChE J.*, Vol. 27, No. 2, pp. 177-184.

25. Herman, G. T., Lakshminarayanan, A. V. and Naperstek, A., 1976, "Convolution Reconstruction Techniques for Divergent Beams", *Computers in Biology and Medicine*, Vol. 6, pp. 259-471.

26. Herman, G. T., Lewitt, R. M., Odhner, D. and Rowland, S. W., 1989, "SNARK89 A Programming System for Image Reconstruction from Projections", University of Pennsylvania, Technical Report No. MIPG160.

27. Hertz, H. M., 1985, "Experimental Determination of 2-D Flame Temperature Fields by Interferometric tomography", *Opt. Comms.*, Vol. 54, pp. 131-135.

28. Hicks, P. J., Narayanan, R. and Deans, H. A., 1990, "An Experimental Study of Miscible Displacements in Heterogeneous Carbonate Cores Using X-Ray CT", *SPEJ* pp. 231-245.

29. Kantzas, A., 1994, "Computation of Holdup in Fluidized and Trickle Beds by Computer Assisted Tomography", *AIChE J.*, Vol. 40, No. 7, pp. 1254-1261.

30. Kumar, B. S., 1994, *Computed Tomographic Measurements of Void Fraction and Modeling of the Flow in Bubble Columns*, Ph.D. Thesis, Florida Atlantic University, Boca Raton, FL.

31. Kumar, B. S., Moslemian, D., and Duduković, M. P., 1995, "A Gamma Ray Tomographic Scanner for Imaging Void Fraction Distribution in Bubble Columns", Flow Meas. Instr., Vol. 6, No. 1, pp. 61-73.

32. Jasti, J., Jesion, G. and Feldkamp, L., 1990, "Microscopic Imaging of Porous Media Using X-Ray Computer Tomography", *SPEJ*, pp. 269-276.

33. Lange, K. and Carson, R., 1984, "EM Reconstruction Algorithms for Emission and Transmission Tomography", *J. Comput. Assist. Tomogr.*, Vol. 8, No. 2, pp. 306-316.

34. Liu, T. C. and Merzkirch, W. and Oberste-Lehn, K., 1989, "Optical Tomography Applied to Speckle Photographic Measurement of Asymmetric Flows with Variable Density", *Experiments in Fluids*, Vol. 7, No. 3, pp. 157-163.

35. Lutran, P. G. and Ng, K. M. and Delikat, E. P., 1991, "Liquid Distribution in Trickle Beds. An Experimental Study Using Computed-Assisted Tomography", *Ind. Engg. Chem. Res.*, Vol. 30, No. 6, pp. 1270-1280.

36. MacAllister, D. J. Miller, K., Graham, S. K. and Yang, C. T., 1990, "Application of X-Ray CT Scanning to the Determination of Gas-Water Relative Permeabilities", *SPEJ*, pp. 255-267.

37. Martz, H. E., Azevedo, S. G., Braske, J. M., Waltjen, K. E. and Schneberk, D. J., 1993, "Computed tomography systems and their industrial applications", *Proc. of American Nucl. Soc., Applied Radiation and Isotopes Measurement and Industrial Applications*, Vol. 41, No. 10-11, pp. 943-961.

38. Newton, T. H. and Potts, D. G., 1981, "Radiology of the Skull and Brain., Vol. 5 : Technical Aspects of Computed Tomography", The C. V. Mosby Co., St. Louis.

39. Peters, T. M. and Lewitt, R. M., 1977, "Computed Tomography with Fan Beam Geometry", *J. Comp. Assist. Tomography*, Vol. 1, No., 4, pp. 429-436.

40. Radon, J., 1917, "Ueber die Bestimmung von Funktionen durch ihre Integralwerte langs gewisser Manningfaltigkeiten", *Berichte Saechsische Akad. Wiss.*, Vol. 69.

41. Schneberk, D. J., Azevedo, S. G. Martz, H. E. and Skeate, M. F., 1990, "Sources of Error in Industrial Tomographic Reconstructions", *Materials Evaluation*, Vol. 48, No. 5, pp. 609-617.

42. Severance, W. A. N., 1981, "Advances in Radiation Scanning of Distillation Columns", *Che. Eng. Prog.*, Vol. 77, N0. 9, pp. 38-41.

43. Severance, W. A. N., 1985, "Differential Radiation Scanning Improves the Visibility of Liquid Distribution", *Che. Eng. Prog.*, Vol. 81, N0. 4, pp. 48-51.

44. Seville, J. P. K., Morgan, J. E. P. and Clift, R., 1986, "Tomographic Determination of the Voidage Structure of Gas Fluidized Beds in the Jet Region", *Fluidization V, Proc. of the 5 th Int. Conf. on Fluidization, Denmark*, pp. 87-93.

45. Shepp, L. A. and Logan, B. F., 1974, "The Fourier Reconstruction of a Head Section", *I. E. E. E., Trans. Nucl. Sci.*, Vol. NS-21, pp. 21.

46. Shepp, L. A. and Stein, J., 1977, "Simulated Reconstruction Artifacts in Computerized X-ray Tomography", in *Reconstruction Tomography in Diagnostic Radiology and Nuclear Medicine*, Ed: M. M. Ter-Pogossian, University Park Press, Baltimore, MD.

47. Simons, S. J. R. and Williams, R. A., 1993, *Powder Technology*, Vol. 73, pp. 85.

48. Stanley, W., 1975, "Digital Signal Processing", Reston Publ. Co., Reston, VA.

49. Swift, W. L., Dolan, F. X. and Runstadler, P. W., 1978, "A Scanning gamma Ray Attenuation System for Void Fraction Measurements in Two-Phase Flow", in *Measurements in Polyphase Flows, Proc. of the Winter Annual Meeting of ASME,* San Francisco, 1978, pp : 25-35.

50. Tsoulfanidis, N., 1983, "Measurement and Detection of Radiation", McGraw Hill, New York.

51. Toye, D., Marchot, P., Crine, M., and Homer, G. L., 1994, "The Use of Large Scale Computer Assisted Tomography for the Study of Hydrodynamics in Trickling Filters", *Che. Eng. Sci.*, Vol. 49, No. 24B, pp. 5271-5280.

52. Watt, D. W. and Vest, C. M., 1990, "Turbulent Flow Visualization by Interferometric Integral Imaging and Computed Tomography", *Experiments in Fluids*, Vol. 8, No. 6, pp. 301-311.

53. White, R. L., 1987, "On-Line Troubleshooting of Chemical Plants", *Che. Eng. Prog.*, Vol. 83, N0.5, pp. 33-38.

54. Wyman, D. R. and Harms, A. A., 1985, "Statistical Uncertainty in the Radiation Diagnosis of Two-Phase Flows", *Nucl. Eng. Des.*, Vol. 85, pp. 261-275.

55. Yester, M. W. and Barnes, G. T., 1977, "Geometrical Limitations of Computed Tomography (C.T.) Scanner Resolution", *Appl. Opt. Instr. in Medicine*, Vol. VI 127, pp. 296-303.

56. Yule, A. J., Ah Seng, C., Felton, P. G., Ungut, A. and Chigier, N. A., 1981, "A Laser Tomographic Investigation of Liquid Fuel Sprays", *Eighteenth International Symposium on Combustion, The Combustion Institute*, pp. 1501-1510.